Applied Physics Letters

Calcium-stannous oxide solid solutions for solar devices

Cite as: Appl. Phys. Lett. **117**, 153901 (2020); https://doi.org/10.1063/5.0024947
Submitted: 12 August 2020 . Accepted: 27 September 2020 . Published Online: 12 October 2020

Ned Thaddeus Taylor, Arnaldo Galbiati, Monica Saavedra, and Steven Paul Hepplestone

Applied Physics Letters ARTICLE scitation.org/journal/apl

Calcium-stannous oxide solid solutions for solar devices

Cite as: Appl. Phys. Lett. **117**, 153901 (2020); doi: 10.1063/5.0024947
Submitted: 12 August 2020 · Accepted: 27 September 2020 ·
Published Online: 12 October 2020

Ned Thaddeus Taylor,[1] Arnaldo Galbiati,[2,a)] Monica Saavedra,[2] and Steven Paul Hepplestone[1,a)]

AFFILIATIONS

[1]School of Physics and Astronomy, University of Exeter, Stocker Road, Exeter EX4 4QL, United Kingdom
[2]Solaris Photonics, St John's Innovation Centre, Cowley Road, Cambridge CB4 0WS, United Kingdom

[a)]**Authors to whom correspondence should be addressed:** admin@solaris-photonics.com and S.P.Hepplestone@exeter.ac.uk

ABSTRACT

In this study, solid solutions formed of SnO and CaO [termed $(Sn:Ca)_xO$] are explored as potential solar active layers. The results indicate that a ratio of $x = 7:1$ leads to a fundamental direct bandgap of 1.56 eV. In order to promote the transport of excited charge carriers from within the active layer, appropriately aligned hole/electron transport layers need to be identified. To this end, a set of results are presented for the electronic band alignment of $(Sn:Ca)_{7:1}O$ with a selection of oxide transport layers, with and without oxygen vacancies. From this, it is recommended that a $CaO/(Sn:Ca)_{7:1}O/TiO_2$ device shows the most potential for an all-oxide solar cell.

Solar cell development is driven by how to design a cheap, large-scale working device. Ideally, this device needs to have an active layer, possessing a 1.34 eV bandgap (related to the Shockley Queisser limit)[1,2] and a built-in field to drive the current. There are two ways to form this field—p–n and p–i–n junctions. Traditional silicon solar cells take advantage of the p–n junction design, but a potentially cheaper alternative is an oxide p–i–n solar cell.[3] However, oxides have been held back by issues such as large bandgaps and oxygen vacancies. The present leading oxide, Cu_2O,[4] is limited to 20% efficiency, due to its bandgap of over 2 eV.

For the p–i–n junction, the band alignment between the various layers (contact, transport, and active) is of vital importance. Typically, the transport layers need to be semiconducting/insulating materials, with band alignments to the active layer exhibiting type II (staggered) structures. This allows for the electrons and holes to be driven in opposite directions, aiding in the separation of the charge carriers.

While silicon is currently the industry leading standard for solar cells (reaching 26.7% efficiency),[5] its manufacturing processes present many issues and limitations.[5–7] These could be overcome by using oxides for all component layers. Oxide versatility stems from their rich array of electronic properties, ease of fabrication,[8,9] as well as sustainability, due to the fact that many of them are formed of abundant, nontoxic elements.

Stannous oxide, SnO, has been explored recently as a candidate for the active layer of oxide solar cells.[10] It has garnered attention due to its highly dispersive conduction bands, anisotropy in effective mass, and its relative ease of fabrication and stability.[11] However, its photovoltaic use is limited due to its small, indirect bandgap (below 0.7 eV).

Optical properties of a material can be improved through solid solution, which consists of mixing two materials with different properties. Thus, it is desirable to mix SnO with a material exhibiting a direct and larger bandgap. Recent works have investigated mixing SnO with calcium oxide, CaO, to increase the bandgap.[10] When forming a solid solution, one of the main questions, after determining the materials to mix, is the proportion of each material to use.

In this work, we present a first principles study of forming solid solutions between SnO and CaO for use as a solar cell active layer. We explore how different mixing ratios affect the electronic properties, as well as their stabilities. We then identify a potential p–i–n solar cell design by exploring contact and electron/hole transport layers (ETLs/HTLs) compatible with our $(Sn:Ca)_xO$ active layer.

In this work, first principles techniques based on Density Functional Theory (DFT) were used to determine structural and electronic properties of the various materials considered for solar cell layers. These calculations were performed using VASP.[12,13] The valence electrons for each atomic species are considered as follows: Ca $3s^2 3p^6 4s^2$, Sn $5s^2 5p^2$, O $2s^2 2p^4$, Ti $3p^6 3d^4 4s^2$, Mo $5s^1 4d^5$, F $2s^2 2p^5$, and Li $1s^2 2s^1$. The projector augmented wave method was used, with an energy cutoff of 700 eV. Bulk structural properties were completed using the PBE functional,[14] while bulk electronic properties were

obtained using the screened-hybrid functional HSE06.[15] As the PBE functional is known to underpredict the bandgap of materials, the HSE06 functional has been employed where it is possible to improve this agreement with experiment. All slab and heterostructure calculations were performed using PBE. Forces were relaxed to less than 0.01 eV/Å per atom, and electronic self-consistency is accurate to within 10^{-7} eV. Our calculations were performed using k-point grids with densities equivalent to those used for analyzing the SnO bulk unit cell, where geometric relaxations and electronic calculations used $6 \times 6 \times 9$ and $12 \times 12 \times 18$ Monkhorst-Pack grids, respectively.[16] For the slab (interface) supercell structures, these were reduced to equivalent $m \times n \times 1$ grids. Electrostatic potential plots were obtained following the method outlined by Delaney *et al.*[17] and Hepplestone and Sushko.[18]

Various phases and termination planes have been explored for materials considered. Here, we present only the phases that resulted in the most energetically favorable interfaces with the active layer. All slab and interface structures are generated using the ARTEMIS software package.[19] For these structures, the following terminations and phases are presented: SnO (001), Ca (001), CaO (101), anatase TiO_2 (001), CaF_2 (101), LiF (001), and α-MoO_3 (001).

To optimize the electronic bandgap, we propose forming a solid solution of the two oxides, SnO and CaO, with the chemical formula $(Sn:Ca)_xO$ (where x defines the Sn:Ca ratio). This optimization consists of increasing the SnO gap and reducing the difference between the direct and indirect transitions.

Figure 1 presents the relationship between the bandgap and the solid solution ratio (x). Solid solution ratios lower than 1:1 exhibit similar bandgaps to each other, within the range of 1.2–1.6 eV (HSE06 values), optimal for photovoltaic applications. We determine that a solid solution with $x = 7:1$ will achieve a fundamental direct bandgap of 1.56 eV at Γ, which is much closer to the optimum bandgap of a single-junction solar cell (1.34 eV) than pure SnO. While a composition of $x = 3{:}1$ exhibits a better bandgap of 1.22 eV, it is strongly indirect, and thus, we focus instead on $x = 7{:}1$. Note that the change in bandgaps caused by the alloying presents itself not as defect states within the bandgap, but instead as alterations to the dispersive bands in both the valence and conduction band regions. This is due to the changes in the periodicity of the material.

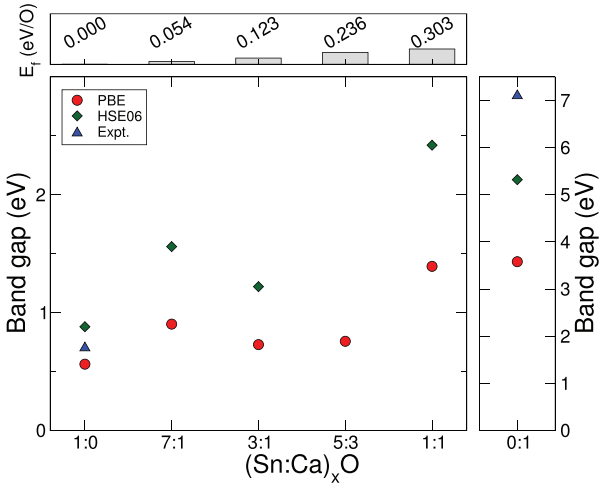

FIG. 1. The dependence of the dopant concentration on the fundamental electronic bandgap size for $(Sn:Ca)_xO$. Where possible, the values obtained using PBE and HSE06 and experimental results have been compared. Experimental bandgaps of SnO and CaO were obtained from Refs. 20 and 21, respectively. The top panel depicts the formation energy of the $(Sn:Ca)_xO$ solid solutions, from PBE, defined as the energy difference between the solid solution and the constituent oxides, normalized by the number of oxygen.

In Fig. 1, we present the energetic cost of forming a solid solution in the α-SnO phase from the constituent oxides SnO and CaO, normalized to the number of oxygen. This is given by

$$E_{f,n:m} = \frac{E_{n:m} - nE_{SnO} - mE_{CaO}}{n+m}, \quad (1)$$

where n (m) represents the number of SnO (CaO) units in the solid solution. The total energies of a single unit of SnO, CaO, and $(Sn:Ca)_{n:m}O$ are denoted as E_{SnO}, E_{CaO}, and $E_{n:m}$, respectively. It is apparent that, as the solid solution approaches $x = 1{:}1$ by increasing the CaO content, the formation energy increases. Hence, for the concentrations studied, the most energetically favorable solid solution in the α-SnO phase is the 7:1 ratio, $E_{f,7:1} = 0.054$ eV per oxygen atom. For all ratios, the elements prefer the individual oxides than the solid solution. However, the formation energy of 7:1 is particularly low, indicating that slight changes in the calcium chemical potential will make this favorable. We also note that the higher the ratio, the more likely that amorphous structures are to form (Fig. 2).

To thoroughly explore the atomic arrangement within the structure, each ratio was allowed to fully relax from the SnO and the CaO atomic geometries. It was found that the SnO geometry was energetically favorable for all concentrations other than 0:1 (pure CaO), however, while the α-SnO phase is found to be more favorable than the rock salt phase (CaO phase) for the solid solutions explored.

Our results show that, as we increase the mix of CaO into SnO, the hole affinity χ_h increases from 4.31 eV in SnO to 4.93 eV for $(Sn:Ca)_{7:1}O$ (see the supplementary material). By increasing the hole affinity of the material, $(Sn:Ca)_{7:1}O$ allows for more oxides to work as hole transport layers. This is due to the preference for oxides to exhibit hole affinities typically greater than 5 eV.[22–24]

Having established a potential photovoltaic active layer, we now explore a set of candidate transport layers for the $(Sn:Ca)_{7:1}O$ solid

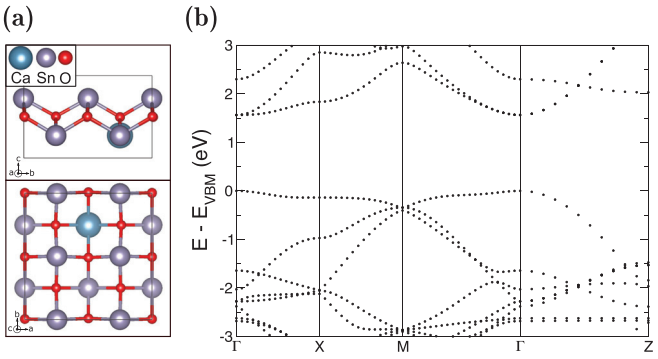

FIG. 2. (a) Ball and stick model of the atomic structure and (b) electronic band structure of $(Sn:Ca)_{7:1}O$, obtained from first principles HSE06 calculations. The shaded region highlights the bandgap of the system. Energies are given relative to the valence band maximum (VBM).

solution to aid in the separation of charge carriers. As it is known that metal Fermi levels are pinned to the oxide HTL and ETL Fermi level,[25] we focus on the alignment of these (the ETL and HTL) with the active $(Sn:Ca)_{7:1}O$ layer. While there is a clear disagreement between the theoretical and experimental bandgaps (even when employing HSE06 to compensate), the qualitative results (relative bandgap sizes) are reproduced and this quantitative discrepancy (exact bandgap sizes) should not be present in theoretical hole affinities. This is because the hole affinities are determined by the occupied states, whose PBE has been shown to be reliable for predicting.[26] As the band alignment should be reasonable, we have provided the experimental bandgaps to allow the reader to consider the true band alignment.

In Table I, we present the hole affinities of SnO, $(Sn:Ca)_{7:1}O$, CaO, TiO_2, CaF_2, LiF, and MoO_3 to compare potential transport layers with the hole affinity of the active layer. In doing so, one can estimate, using Schottky–Mott prediction,[31] whether a material is more suitable for hole or electron transport; however, this does not account for changes in band alignment due to interfacial effects.[19] Thus, this method provides an initial screening method to select suitable candidate materials for further studies. Hence, using the table alongside the previous criteria for identifying electron and hole transport layers, we can determine that CaO should act as hole transport layers, while MoO_3 should be the only viable electron transport layer from the list. The other potential transport layers straddle the bandgap of the active layer, which would force both charge carrier types to flow away from the transport layer. Note that due to the intrinsic n-type dopant state of TiO_2 (caused by inherent oxygen vacancies[32]), it is possible that this layer could act as a transport layer.

We first explore these heterostructures without intrinsic dopants, such as oxygen vacancies (discussed later). This allows us to determine the idealized alignment of these materials and whether this is desirable. We now present, in Table II, a comparison between the exact calculated value from DFT and the previously discussed Schottky–Mott prediction for band alignment. While some band alignments show little change—$(Sn:Ca)_{7:1}O/CaO$ and $(Sn:Ca)_{7:1}O/CaF_2$—some show drastic changes—$(Sn:Ca)_{7:1}O/TiO_2$ and $(Sn:Ca)_{7:1}O/MoO_3$. Most of these candidate materials exhibit valence band maxima below and bandgaps larger than that of the active layer. This leads to type I (straddled) band alignment occurring in many of the potential electron transport layer candidates. From Tables I and II, it is apparent that both hole and electron transport layers are challenging to find for $(Sn:Ca)_{7:1}O$. Hole transport layers are limited by the higher chance of oxides to exhibit hole affinities greater than 5 eV, while the problem in finding electron transport layers is linked to the large bandgaps (> 2 eV) typical of oxides.

TABLE I. Theoretical hole affinities and bandgaps of various undoped materials. Experimental bandgaps (where available) are presented for comparison. These materials are considered for their potential as active and transport layers. TiO_2 is presented in the anatase phase. Hole affinities and theoretical bandgap values are obtained from first principles PBE calculations.

Layer	Material	χ_h (eV)	$E_{g,\text{theory}}$ (eV)	$E_{g,\text{expt}}$ (eV)
Active layers	SnO	4.31	0.56	0.7[20]
	$(Sn:Ca)_{7:1}O$	4.93	0.90	1.56[a]
Transport layers	CaO	4.09	3.58	7.1[21]
	TiO_2	6.20	2.04	3.4[27]
	CaF_2	6.69	7.38	11.2[28]
	LiF	7.68	9.39	13.6[29]
	MoO_3	8.50	1.73	3.1[30]

[a]HSE06 result.

TABLE II. Predicted and calculated band alignments of a set of materials against $(Sn:Ca)_{7:1}O$. Predicted values are obtained by comparing the hole affinities of the two materials, the Schottky–Mott method. Calculated values are obtained from the electrostatic potential of the interface structure consisting of the two materials. Positive (negative) values represent materials having valence band maxima above (below) those of the active layer. Results are obtained from first principles PBE calculations.

	Band alignment (eV)	
Material	Predicted	Calculated
Ca	2.17	1.15
CaO	0.84	0.92
TiO_2	−1.27	−0.17
CaF_2	−1.76	−1.74
LiF	−2.75	−3.15
MoO_3	−3.75	−1.47

Figure 3 depicts the band alignment between $(Sn:Ca)_{7:1}O$ and a set of potential transport layers (CaO, MoO_3, and TiO_2) as well as Ca (see the supplementary material for a comparison to bulk properties). Here, the band alignment is defined as the difference between the valence band maxima (Fermi energy for metals) of the two materials (for further details, see the supplementary material). From the density of states for each of the heterostructures, it becomes apparent that interface states arise at the $(Sn:Ca)_{7:1}O$ slab surface, with similar effects occurring on the surface of the neighboring transport layer. For some systems, these are less apparent—such as with the $(Sn:Ca)_{7:1}O/Ca$ heterostructure—whereas others show rather pronounced changes—as is the case with the $(Sn:Ca)_{7:1}O/TiO_2$ heterostructure.

The inclusion of Ca in this study is due to the intriguing features it exhibits in its density of states when in a heterostructure with $(Sn:Ca)_{7:1}O$. The exploration here is as a potential contact directly on the active layer. The band alignment between $(Sn:Ca)_{7:1}O$ and Ca is found to be 1.15 eV. The disparity in the density of states and the lack of states available near the $(Sn:Ca)_{7:1}O$ valence bands should allow for a biased transport of the carriers. Furthermore, this disparity in available electron and hole states could lead to a higher number of electron carriers compared to holes. However, without a detailed experimental study of the conductivity of the interface structure, this cannot be confirmed. Note that this setup could lead to further issues as a metal-on-metal oxide heterostructure could risk the formation of a CaO insulator at the interface. While this point is of high interest, we now focus on the traditional p–i–n approach and disregard a direct Ca contact. With this in mind, we now discuss CaO as a potential transport layer.

The band alignment between $(Sn:Ca)_{7:1}O$ and CaO is 0.92 eV. This results in the valence bands of CaO lying close to the conduction band of the active layer. The large bandgap of CaO causes its conduction states to lie far above that of the active layer. This is a Type II band alignment. From the results presented here, CaO appears to be a

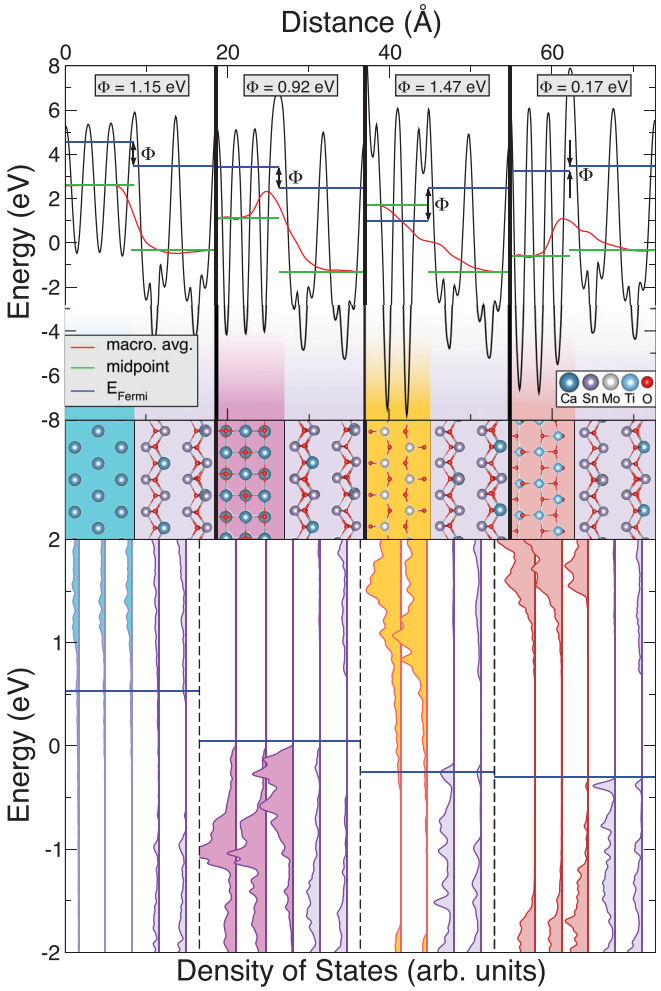

FIG. 3. (top) Electrostatic potential, (middle) ball and stick model of the atomic structure, and (bottom) layer-projected density of states of (left to right) $(Sn:Ca)_{7:1}O/Ca$, $(Sn:Ca)_{7:1}O/CaO$, $(Sn:Ca)_{7:1}O/MoO_3$, and $(Sn:Ca)_{7:1}O/TiO_2$ heterostructures, obtained from first principles PBE calculations. Φ denotes the band alignment of each heterostructure. The electronic states are aligned to the core states of the $(Sn:Ca)_{7:1}O$ slab-center layers. The blue lines in both the top and bottom panels denote the Fermi energy in the respective region. The bold (dashed) lines in the local potentials (density of states) separate the different heterostructures that have been modeled.

suitable candidate for the hole transport layer (potentially with Ca as the metal contact).

For the electron transport layer, there are two candidates we consider: MoO_3 and TiO_2. MoO_3 and $(Sn:Ca)_{7:1}O$ have a band alignment of 1.47 eV, while TiO_2 and $(Sn:Ca)_{7:1}O$ show a band alignment of 0.17 eV. The valence band maxima and conduction band minima of both transport layers lie below and above those of the active layer, respectively—this results in type I band alignment. In the $(Sn:Ca)_{7:1}O/MoO_3$ heterostructure, there are a large offset between the valence bands, effectively creating a large barrier for holes, and a small offset between the conduction bands, indicating a minor effect on the electrons. This could lead to a strong separation of the charge carriers. In the $(Sn:Ca)_{7:1}O/TiO_2$ heterostructure, the opposite features are seen, where the hole has only a small offset in the valence bands, while the conduction band offset for electrons is much more pronounced. For these defect-free heterostructures, $CaO/(Sn:Ca)_{7:1}O/MoO_3$ and $CaO/(Sn:Ca)_{7:1}O/TiO_2$ are shown to be viable solar cell designs. However, for a full consideration, the effects of oxygen vacancies on MoO_3 and TiO_2 need to be considered.

Most oxides are known to be intrinsically doped with oxygen vacancies. These lead to binary and ternary oxides being n-type doped and monoxides being p-type doped. The doping can lead to radical changes in the band alignment. While oxygen vacancies have been explored in both candidate electron transport layers, the band alignment in the $CaO/(Sn:Ca)_{7:1}O/MoO_3$ heterostructure remains relatively unaffected (see the supplementary material). Hence, the discussion ahead focuses solely on the $CaO/(Sn:Ca)_{7:1}O/TiO_2$ solar cell design.

To consider the effects of oxygen vacancies in potential all-oxide solar cell setups, we model an equivalent concentration of 1 oxygen vacancy present per 24 TiO_2 unit (1.19×10^{21} cm^{-3}). While this concentration is much higher than that would likely exist in a physical system, it represents the highest potential effect of oxygen vacancies on the band alignment (see the supplementary material for further details).

Figure 4 depicts the effect of an oxygen vacancy in the $CaO/(Sn:Ca)_{7:1}O/TiO_2$ heterostructure, with the vacancy having been placed near the center of the TiO_2 region. As can be seen, the introduction of an oxygen vacancy into the TiO_2 region results in n-type doping, in agreement with experiment.[23,33] This doping results in two

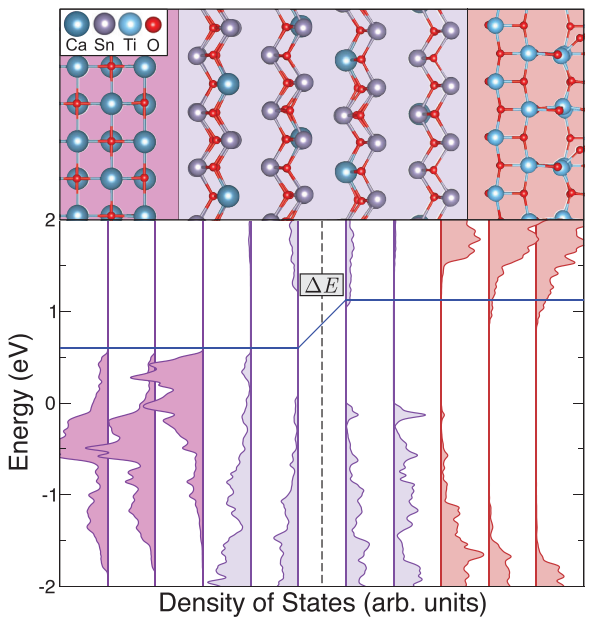

FIG. 4. (top) Ball and stick model of the atomic structure and (bottom) layer-projected density of states of $CaO/(Sn:Ca)_{7:1}O$ and $(Sn:Ca)_{7:1}O/TiO_2$, obtained from first principles PBE calculations. An oxygen vacancy is present in the center of the TiO_2 region. The electronic states are aligned to the core states of the $(Sn:Ca)_{7:1}O$ slab-center layers. The blue lines denote the Fermi energy in each system. ΔE defines the difference between the Fermi energies (0.525 eV).

main changes to the density of states. First, the TiO_2 material gains shallow n-type dopant states in the bandgap. Second, the alignment of the density of states associated with the TiO_2 region is seen to be lower in energy by about 0.5 eV with respect to the defect-free TiO_2 region. This means that the inclusion of oxygen vacancies makes TiO_2 a more viable electron transport layer for the active layer of $(Sn:Ca)_{7:1}O$. From this, we can see that the offset in the Fermi levels between the $(Sn:Ca)_{7:1}O/CaO$ and $(Sn:Ca)_{7:1}O/TiO_2$ regions is 0.525 eV, which would lead to a strong driving field to form across a device with this setup.

We now present a potential setup for an all-oxide solar cell with $(Sn:Ca)_{7:1}O$ as the active layer, taking into account the effects of oxygen vacancies. This setup is $CaO/(Sn:Ca)_{7:1}O/TiO_2$, which presents a favorable alignment of the bands such that a driving field should be present over the system. We suggest that this system is explored further as a potentially viable all-oxide solar cell design, with an effective energy shift of 0.525 eV.

Here, we have explored the potential of doping SnO to improve its electronic properties for photovoltaic applications. It is found that a solid solution formed of SnO and CaO at a ratio of 7:1 results in the bandgap of SnO changing from indirect to direct and increasing the fundamental gap to 1.56 eV. Furthermore, the SnO structure shows strong thermal stability and anisotropic conduction properties. With all these capabilities, the solid solution $(Sn:Ca)_{7:1}O$ has the promise to be an efficient photovoltaic material.

However, while the electronic properties of the solid solution $(Sn:Ca)_{7:1}O$ make it an intriguing candidate as an active layer in oxide solar cells, the poor band alignment between many other oxides makes it challenging to identify a suitable transport layer. Overall, CaO should be a viable hole transport layer due to its capability to sustain p-type doping and appropriate band alignment with the active layer. For the electron transport layer, we see that TiO_2 is a promising candidate and, from preliminary studies, find that its intrinsic n-type doping should make it even more suitable. Thus, we recommend that a $CaO/(Sn:Ca)_{7:1}O/TiO_2$ device shows the most potential for an all-oxide solar cell, which could offer an improvement in performance, due to the direct bandgap of 1.56 eV.

See the supplementary material for further details on the methods used for determining band alignment and the bulk properties of the oxides, fluorides, and metals considered here. The energetic, electronic, and geometric properties of the solid solutions are also discussed in further detail, along with their surface properties. Finally, the $(Sn:Ca)_{7:1}O/MoO_3$ heterostructure is explored further, including oxygen vacancies in the system.

Via our membership of the UK's HEC Materials Chemistry Consortium, which was funded by EPSRC (Nos. EP/L000202 and EP/R029431), this work used the ARCHER UK National Supercomputing Service (http://www.archer.ac.uk). This work used the Isambard UK National Tier-2 HPC Service (http://gw4.ac.uk/isambard/) operated by GW4 and the UK Met Office and funded by EPSRC (No. EP/P020224/1). Also, all the authors acknowledge funding from the EPSRC (No. EP/L015331/1). This work was made possible due to funding from Solaris Photonics. Finally, the authors thank Francis Huw Davies for his useful discussions.

DATA AVAILABILITY

The data that support the findings of this study are openly available from the University of Exeter's Institutional repository at https://doi.org/10.24378/exe.2663, Ref. 34.

REFERENCES

[1]W. Shockley and H. J. Queisser, "Detailed balance limit of efficiency of p–n junction solar cells," J. Appl. Phys. **32**(3), 510–519 (1961).
[2]S. Rühle, "Tabulated values of the Shockley-Queisser limit for single junction solar cells," Sol. Energy **130**, 139–147 (2016).
[3]S. Rühle, A. Y. Anderson, H. Noa Barad, B. Kupfer, Y. Bouhadana, E. Rosh-Hodesh, and A. Zaban, "All-oxide photovoltaics," J. Phys. Chem. Lett. **3**(24), 3755–3764 (2012).
[4]T. Dimopoulos, *All-Oxide Solar Cells* (Elsevier Inc., 2018).
[5]P. K. Nayak, S. Mahesh, H. J. Snaith, and D. Cahen, "Photovoltaic solar cell technologies: Analysing the state of the art," Nat. Rev. Mater. **4**(4), 269–285 (2019).
[6]S. Dubey, N. Y. Jadhav, and B. Zakirova, "Socio-economic and environmental impacts of silicon based photovoltaic (PV) technologies," Energy Procedia **33**, 322–334 (2013).
[7]H. J. Tchognia Nkuissi, F. Kouadio Konan, B. Hartiti, and J.-M. Ndjaka, "Toxic Materials used in thin film photovoltaics and their impacts on environment," *Reliability and Ecological Aspects of Photovoltaic Modules*, (IntechOpen, 2020), pp. 1–18.
[8]M. Coll, J. Fontcuberta, M. Althammer, M. Bibes, H. Boschker, A. Calleja, G. Cheng, M. Cuoco, R. Dittmann, B. Dkhil, I. E. Baggari, M. Fanciulli, I. Fina, E. Fortunato, C. Frontera, S. Fujita, V. Garcia, S. T. B. Goennenwein, C. G. Granqvist, J. Grollier, R. Gross, A. Hagfeldt, G. Herranz, K. Hono, E. Houwman, M. Huijben, A. Kalaboukhov, D. J. Keeble, G. Koster, L. F. Kourkoutis, J. Levy, M. Lira-Cantu, J. L. MacManus-Driscoll, J. Mannhart, R. Martins, S. Menzel, T. Mikolajick, M. Napari, M. D. Nguyen, G. Niklasson, C. Paillard, S. Panigrahi, G. Rijnders, F. Sánchez, P. Sanchis, S. Sanna, D. G. Schlom, U. Schroeder, K. M. Shen, A. Siemon, M. Spreitzer, H. Sukegawa, R. Tamayo, J. van den Brink, N. Pryds, and F. Miletto Granozio, "Towards oxide electronics: A roadmap," Appl. Surf. Sci. **482**, 1–93 (2019).
[9]N. T. Taylor, F. H. Davies, S. G. Davies, C. J. Price, and S. P. Hepplestone, "The fundamental mechanism behind colossal permittivity in oxides," Adv. Mater. **31**(51), 1904746 (2019).
[10]H. Peng, A. Bikowski, A. Zakutayev, and S. Lany, "Pathway to oxide photovoltaics via band-structure engineering of SnO," APL Mater. **4**(10), 106103 (2016).
[11]K. Niwa, I. Yamai, and T. Wada, "A study of tin oxides by x-ray diffraction method," Bull. Chem. Soc. Jpn. **31**(6), 725–727 (1958).
[12]G. Kresse and J. Furthmüller, "Efficient iterative schemes for ab initio total-energy calculations using a plane-wave basis set," Phys. Rev. B **54**(16), 11169–11186 (1996).
[13]G. Kresse and J. Furthmüller, "Efficiency of ab-initio total energy calculations for metals and semiconductors using a plane-wave basis set," Comput. Mater. Sci. **6**(1), 15–50 (1996).
[14]J. P. Perdew, K. Burke, and M. Ernzerhof, "Generalized gradient approximation made simple," Phys. Rev. Lett. **77**(18), 3865–3868 (1996).
[15]A. V. Krukau, O. A. Vydrov, A. F. Izmaylov, and G. E. Scuseria, "Influence of the exchange screening parameter on the performance of screened hybrid functionals," J. Chem. Phys. **125**(22), 224106 (2006).
[16]H. J. Monkhorst and J. D. Pack, "Special points for Brillouin-zone integrations," Phys. Rev. B **13**(12), 5188–5192 (1976).
[17]K. T. Delaney, N. A. Spaldin, and C. G. Van De Walle, "Theoretical study of Schottky-barrier formation at epitaxial rare-earth-metal/semiconductor interfaces," Phys. Rev. B **81**(16), 165312 (2010).
[18]S. P. Hepplestone and P. V. Sushko, "Effect of metal intermixing on the Schottky barriers of Mo(100)/GaAs(100) interfaces," J. Appl. Phys. **116**(19), 193703 (2014).
[19]N. T. Taylor, F. H. Davies, I. EdwardMikel Rudkin, C. J. Price, T. H. Chan, and S. P. Hepplestone, "ARTEMIS: Ab initio restructuring tool enabling the modelling of inter face structures," Comput. Phys. Commun. **257**, 107515 (jul 2020)page.

[20]Y. Ogo, H. Hiramatsu, K. Nomura, H. Yanagi, T. Kamiya, M. Hirano, and H. Hosono, "p-channel thin-film transistor using p-type oxide semiconductor, SnO," Appl. Phys. Lett. **93**(3), 032113 (2008).
[21]R. C. Whited, C. J. Flaten, and W. C. Walker, "Exciton thermoreflectance of MgO and CaO," Solid State Commun. **13**(11), 1903–1905 (1973).
[22]M. Batzill, "Fundamental aspects of surface engineering of transition metal oxide photocatalysts," Energy Environ. Sci. **4**(9), 3275–3286 (2011).
[23]T. Mark and Z. H. Greiner, "Lu. Thin-film metal oxides in organic semiconductor devices: Their electronic structures, work functions and interfaces," NPG Asia Mater. **5**(7), e55 (2013).
[24]J. Kim, K. Yamamoto, S. Iimura, S. Ueda, and H. Hosono, "Electron affinity control of amorphous oxide semiconductors and its applicability to organic electronics," Adv. Mater. Interfaces **5**(23), 1801307 (2018).
[25]L. R. Fonseca, A. A. Knizhnik, A. V. Gavrikov, I. M. Iskandarova, A. A. Bagatur'yants, and B. V. Potapkin, "Fermi pinning in metal-oxide-semiconductor structures results from low oxygen content at the metal-oxide interface," in ECS Transactions (ECS, 2007), Vol. 4, pp. 227–235.
[26]M. Ernzerhof and G. E. Scuseria, "Assessment of the Perdew-Burke-Ernzerhof exchange-correlation functional," J. Chem. Phys. **110**(11), 5029–5036 (mar1999).
[27]H. Tang, F. Lévy, H. Berger, and P. E. Schmid, "Urbach tail of anatase TiO_2," Phys. Rev. B **52**(11), 7771–7774 (1995).
[28]G. W. Rubloff, "Far-ultraviolet reflectance spectra and the electronic structure of ionic crystals," Phys. Rev. B **5**(2), 662–684 (1972).
[29]D. M. Roessler and W. C. Walker, "Electronic spectrum of crystalline lithium fluoride," J. Phys. Chem. Solids **28**(8), 1507–1515 (1967).
[30]M. Kröger, S. Hamwi, J. Meyer, T. Riedl, W. Kowalsky, and A. Kahn, "Role of the deep-lying electronic states of MoO_3 in the enhancement of hole-injection in organic thin films," Appl. Phys. Lett. **95**(12), 123301 (2009).
[31]J. Bardeen, "Surface states and rectification at a metal semi-conductor contact," Phys. Rev. **71**(10), 717–727 (1947).
[32]X. Pan, M. Q. Yang, X. Fu, N. Zhang, and Y. J. Xu, "Defective TiO_2 with oxygen vacancies: Synthesis, properties and photocatalytic applications," Nanoscale **5**(9), 3601–3614 (2013).
[33]B. J. Morgan and G. W. Watson, "Intrinsic n-type defect formation in TiO_2: A comparison of rutile and anatase from GGA+U calculations," J. Phys. Chem. C **114**(5), 2321–2328 (2010).
[34]N. T. Taylor, A. Galbiati, M. Saavedra, and S. P. Hepplestone (2020). "Calcium-stannous oxide solid solutions for solar devices (dataset)" University of Exeter's Institutional, https://doi.org/10.24378/exe.2663.